

# Phase estimation via number-conserving operation inside the SU(1,1) interferometer

Qingqian Kang<sup>1,2</sup>, Zekun Zhao<sup>1</sup>, Teng Zhao<sup>1</sup>, Cunjin Liu<sup>1</sup>, and Liyun Hu<sup>1,3\*</sup>

<sup>1</sup>Center for Quantum Science and Technology, Jiangxi Normal University, Nanchang 330022, China

<sup>2</sup>Department of Physics, Jiangxi Normal University Science and Technology College, Nanchang 330022, China

<sup>3</sup>Institute for Military-Civilian Integration of Jiangxi Province, Nanchang 330200, China

Utilizing nonlinear elements, SU(1,1) interferometers demonstrate superior phase sensitivity compared to passive interferometers. However, the precision is significantly impacted by photon losses, particularly internal losses. We propose a theoretical scheme to improve the precision of phase measurement using homodyne detection by implementing number-conserving operations ( $aa^\dagger$  and  $a^\dagger a$ ) within the SU(1,1) interferometer, with the coherent state and the vacuum state as the input states. We analyze the effects of number-conserving operations on the phase sensitivity, the quantum Fisher information, and the quantum Cramér-Rao bound under both ideal and photon losses scenarios. Our findings reveal that the internal non-Gaussian operations can enhance the phase sensitivity and the quantum Fisher information, and effectively improve the robustness of the SU(1,1) interferometer against internal photon losses. Notably, the  $aa^\dagger$  scheme exhibits superior improvement in both ideal and photon losses cases in terms of phase sensitivity. Moreover, in the ideal case,  $aa^\dagger$  scheme slightly outperforms  $a^\dagger a$  scheme in terms of the quantum Fisher information and the Quantum Cramér-Rao. However, in the presence of photon losses,  $a^\dagger a$  scheme demonstrates a greater advantage.

PACS: 03.67.-a, 05.30.-d, 42.50.Dv, 03.65.Wj

## I. INTRODUCTION

Optical interference measurement plays a crucial role in many scientific and technological applications such as quantum metrology for precise measurements, imaging for capturing detailed visual information, sensing for detecting and measuring physical quantities, and information processing for manipulating and transmitting data [1–9]. Consequently, there has been extensive research and significant advancements in the field of optical interference measurement. To satisfy the need for high precision, a variety of optical interferometers have been proposed and developed. One of the most practical interferometers is the Mach-Zehnder interferometer (MZI), whose phase sensitivity is limited by the standard quantum-noise limit (SQL)  $\Delta\phi = 1/\sqrt{N}$  ( $N$  is the average number of photons within the interferometer), together with solely classical resources as the input of the MZI [10]. Over recent decades, various schemes have been proposed to improve the phase sensitivity of the traditional MZI [11, 12]. It has been demonstrated that the quantum states as the input states to make the traditional MZI beat the SQL. For example, NOON state [13, 14], twin Fock state [15], and the squeezed state [16, 17] *et al* can achieve or even exceed the Heisenberg limit (HL)  $\Delta\phi = 1/N$  [18, 19].

Another possibility to realize quantum-enhanced phase sensitivity is the SU(1,1) interferometer [20, 21], which replaced traditional linear beam splitters (BSs) with optical parametric amplifiers (OPAs). It splits and mixes beams using nonlinear transformations, which is first proposed by Yurke *et al.* [22]. In the SU(1,1) interferometer comprising two OPAs, the first OPA serves

the dual purpose of acquiring entangled resources and suppressing amplified noise. Meanwhile, the subsequent use of the second OPA can lead to signal enhancement, offering a viable pathway for achieving higher precision in phase estimation. By utilizing entangled photon states, the SU(1,1) interferometer can surpass the SQL, enabling higher precision. This technique revolutionized phase estimation, becoming a vital tool in quantum precision measurements. Then, there has been significant interest in studying the SU(1,1) interferometer [23–25]. For instance, Hudelist *et al.* demonstrated that the gain effect of OPA results in the SU(1,1) interferometer exhibiting higher sensitivity compared to traditional linear interferometers [27]. In 2011, Jing *et al.* [28] successfully implemented this interferometer experimentally. In this nonlinear interferometer, the maximum output intensity can be much higher than that of linear interferometer due to the OPA. Apart from the standard form, various configurations of SU(1,1) interferometer have also been proposed [24, 29–37].

As previously mentioned, although SU(1,1) interferometer is highly valuable for precision measurement [38, 39], the precision is still affected by dissipation, particularly photon losses inside the interferometer [40, 41]. Consequently, to further enhance precision, non-Gaussian operations should serve as an effective approach to mitigate internal dissipation. Most theoretical [42–45] and experimental [46–48] studies have fortunately indicated that non-Gaussian operations, such as photon subtraction (PS), photon addition (PA), photon catalysis (PC), quantum scissor and their coherent superposition, are effectively enhancing the nonclassicality and entanglement degrees of quantum states, thereby enhancing their potential in quantum information processing [49, 50]. Experimental studies have illustrated the conditional generation of superpositions of distinct quantum operations through single-photon in-

\* hlyun@jxnu.edu.cn

interference, providing a practical approach for preparing non-Gaussian operations [51]. This advancement has unveiled new possibilities in quantum state manipulation and implications for various quantum technologies. In Ref. [45], Zhang *et al.* proposed a theoretical scheme to improve the resolution and precision of phase measurement with parity detection by using a nonclassical state generated by applying a number-conserving generalized superposition of products (GSP) operation on a two-mode squeezed vacuum state as the input of the MZI. Interestingly, under the same parameters, the phase sensitivity with the GSP operation, in the presence of photon losses can be better than that of both the photon subtraction operation and photon addition operation. Additionally, Xu *et al.* examined the phase sensitivity of SU(1,1) interferometers with internal photon losses and determined that performing photon addition operations internally provides superior results compared to those at the input [52]. Thus, can the internal non-Gaussian operations effectively suppress the influence of noise?

Therefore, in this paper, we concentrate on employing the number-conserving operation (NCO) scheme inside the SU(1,1) interferometer to enhance the measurement accuracy, and then analyze the improvement effect of internal non-Gaussian operations on the phase sensitivity and the quantum Fisher information (QFI) in the presence of photon losses. The remainder of this paper is arranged as follows. Sec. II outlines the theoretical model of the NCO. Sec. III delves into phase sensitivity, encompassing both the ideal case and the internal photon losses case. Sec. IV centers on the QFI and quantum Cramér-Rao bound (QCRB) [53, 54]. Finally, Sec. V provides a comprehensive summary.

## II. MODEL

This section begins with an introduction to the SU(1,1) interferometer, as illustrated in Fig. 1(a). The SU(1,1) interferometer typically consists of two OPAs and a linear phase shifter, making it one of the most commonly used interferometers in quantum metrology research. The first OPA is characterized by a two-mode squeezing operator  $U_{S_1}(\xi) = \exp(\xi_1^* ab - \xi_1 a^\dagger b^\dagger)$ , where  $a$  and  $b$ ,  $a^\dagger$  and  $b^\dagger$  represent the photon annihilation and creation operators, respectively. The squeezing parameter  $\xi_1$  can be expressed as  $\xi_1 = g_1 e^{i\theta_1}$ , where  $g_1$  represents the gain factor and  $\theta_1$  represents the phase shift. This parameter plays a critical role in shaping the interference pattern and determining the system's phase sensitivity. Following the first OPA, mode  $a$  undergoes a phase shift process  $U_\phi = \exp[i\phi(a^\dagger a)]$ , while mode  $b$  remains unchanged. Subsequently, the two beams are coupled in the second OPA with the operator  $U_{S_2}(\xi) = \exp(\xi_2^* ab - \xi_2 a^\dagger b^\dagger)$ , where  $\xi_2 = g_2 e^{i\theta_2}$  and  $\theta_2 - \theta_1 = \pi$ . In this paper, we set the parameters  $g_1 = g_2 = g$ ,  $\theta_1 = 0$ ,  $\theta_2 = \pi$ . We utilize

the coherent state  $|\alpha\rangle_a$  and the vacuum state  $|0\rangle_b$  as input states, and homodyne detection is employed on the mode  $a$  of the output.

The SU(1,1) interferometer is generally susceptible to photon losses, particularly in the case of internal losses. To simulate photon losses, the use of fictitious BSs is proposed, as depicted in Fig. 1(a). The operators of these fictitious BSs can be represented as  $U_B = U_{B_a} \otimes U_{B_b}$ , with  $U_{B_a} = \exp[\theta_a (a^\dagger a_v - a a_v^\dagger)]$  and  $U_{B_b} = \exp[\theta_b (b^\dagger b_v - b b_v^\dagger)]$ , where  $a_v$  and  $b_v$  represent vacuum modes. Here,  $T_k$  ( $k = a, b$ ) denotes the transmissivity of the fictitious BSs, associated with  $\theta_k$  through  $T_k = \cos^2 \theta_k \in [0, 1]$ . The value of transmittance equal to 1 ( $T_k = 1$ ) corresponds to the ideal case without photon losses [52]. In an expanded space, the expression for the output state of the standard SU(1,1) interferometer can be represented as the following pure state, i.e.,

$$|\Psi_{out}^0\rangle = U_{S_2} U_\phi U_B U_{S_1} |\alpha\rangle_a |0\rangle_b |0\rangle_{a_v} |0\rangle_{b_v}. \quad (1)$$

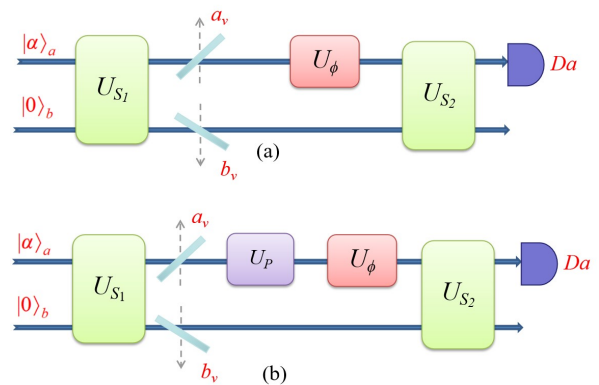


FIG. 1. Schematic diagram of the SU(1,1) interferometer. (a) the standard SU(1,1) interferometer, (b) the SU(1,1) interferometer with NCO. The two input ports are a coherent state  $|\alpha\rangle_a$  and a vacuum state  $|0\rangle_b$ .  $a_v$  and  $b_v$  are vacuum modes.  $U_{S_1}$  and  $U_{S_2}$  are the optical parametric amplifier,  $U_\phi$  is the phase shifter.  $U_P$  is the number-conserving operation and  $D_a$  is the homodyne detector.

To mitigate the impact of photon losses, we introduce a distinct non-Gaussian operation inside the SU(1,1) interferometer, i.e., after the first OPA, called the NCO scheme, as illustrated in Fig. 1(b). As referred to Ref. [45], this NCO can be seen as an equivalent operator,

$$U_P = s a a^\dagger + t a^\dagger a, \quad (2)$$

where  $s + t = 1$ ,  $a$  and  $a^\dagger$  are annihilation operator and creation operator, respectively. It should be emphasized that for simplicity we only consider two cases,  $s = 1$  and  $s = 0$ . From Eq. (2), one can obtain the photon addition then photon subtraction (PA-then-PS)  $a a^\dagger$ , and photon subtraction then photon addition (PS-then-PA)  $a^\dagger a$ , respectively. The process can be described by operators  $U_{P_1} = a a^\dagger$ , and  $U_{P_2} = a^\dagger a$ , respectively. In this case, the

output state of the interferometer can be written as the following pure states

$$|\Psi_{out}^1\rangle = A_1 U_{S_2} U_\phi U_{p_1} U_B U_{S_1} |\alpha\rangle_a |0\rangle_b |0\rangle_{a_v} |0\rangle_{b_v}, \quad (3)$$

and

$$|\Psi_{out}^2\rangle = A_2 U_{S_2} U_\phi U_{p_2} U_B U_{S_1} |\alpha\rangle_a |0\rangle_b |0\rangle_{a_v} |0\rangle_{b_v}. \quad (4)$$

$A_1$  and  $A_2$  are the normalization constants for the PA-then-PS and PS-then-PA, respectively, given by [52]

$$A_1 = (P_{2,2,0,0} + 3P_{1,1,0,0} + 1)^{-\frac{1}{2}}, \quad (5)$$

$$A_2 = (P_{2,2,0,0} + P_{1,1,0,0})^{-\frac{1}{2}}, \quad (6)$$

where  $P_{x_1, y_1, x_2, y_2} = \partial^{x_1+y_1+x_2+y_2} / \partial \lambda_1^{x_1} \partial \lambda_2^{y_1} \partial \lambda_3^{x_2} \partial \lambda_4^{y_2} \{e^{w_4}\}_{\lambda_1=\lambda_2=\lambda_3=\lambda_4=0}$ , as well as

$$w_1 = \lambda_1 T \sinh r (\lambda_2 \sinh r - \lambda_3 \cosh r) + \lambda_4 T \sinh r (\lambda_3 \sinh r - \lambda_2 \cosh r), \quad (7)$$

$$w_2 = \lambda_1 \sqrt{T} \cosh r - \lambda_4 \sqrt{T} \sinh r, \quad (8)$$

$$w_3 = \lambda_2 \sqrt{T} \cosh r - \lambda_3 \sqrt{T} \sinh r, \quad (9)$$

$$w_4 = w_1 + w_2 \alpha^* + w_3 \alpha. \quad (10)$$

### III. PHASE SENSITIVITY

Quantum metrology is an effective approach utilizing quantum resources for precise phase measurements [55, 56]. The objective is to achieve highly sensitive measurements of unknown phases. Within this section, we delve further into investigating the phase sensitivity for the NCO within the SU(1,1) interferometer [57]. Various detection methods are available for this purpose, such as homodyne detection [58, 59], parity detection [60, 61], and intensity detection [62]. Each of these methods offers different trade-offs between sensitivity, complexity, and practical implementation. It is important to note that the phase sensitivities of different detection schemes may vary for different input states and interferometers [63].

Homodyne detection is chosen as the method to detect the output  $a$ , mainly due to its straightforward experimental implementation. In homodyne detection, the measured variable is one of the two orthogonal components of the mode  $a$ , given as  $X = (a + a^\dagger)/\sqrt{2}$ . Based on the error propagation equation [22], the phase sensitivity can be expressed as

$$\Delta\phi = \frac{\sqrt{\langle \Delta^2 X \rangle}}{|\partial \langle X \rangle / \partial \phi|} = \frac{\sqrt{\langle X^2 \rangle - \langle X \rangle^2}}{|\partial \langle X \rangle / \partial \phi|}. \quad (11)$$

Based on Eqs. (3), (4) and (11), the phase sensitivity for the NCO can be theoretically determined. The detail calculation steps for the phase sensitivity  $\Delta\phi$  of the PA-then-PS and PS-then-PA are provided in Appendix A.

#### A. Ideal case

Initially, we consider the ideal case,  $T_k = 1$  (where  $k = a, b$ ), representing the scenario without photon losses. The phase sensitivity  $\Delta\phi$  is plotted as a function of  $\phi$  in Fig. 2. The observations from Fig. 2 can be summarized as follows. (i) The phase sensitivity improves initially and then decreases as the phase increases, with the optimal sensitivity deviating from  $\phi = 0$ . (ii) Both PA-then-PS and PS-then-PA schemes within the SU(1,1) interferometer effectively enhance the phase sensitivity  $\Delta\phi$ . (iii) It is clear that the PA-then-PS scheme outperforms the PS-then-PA scheme at small phase values, while the opposite is true at large phase values. (iv) And the optimal phase sensitivity is obtained in the PA-then-PS scheme, rather than the PS-then-PA scheme.

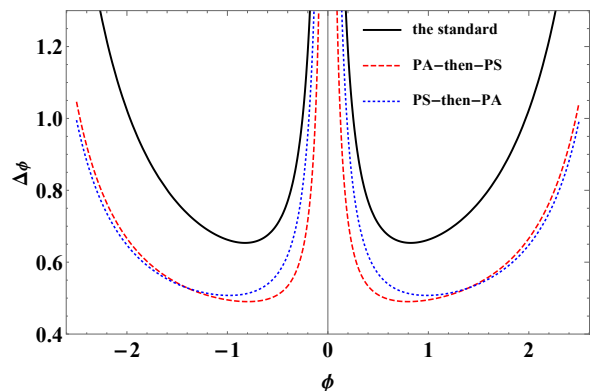


FIG. 2. The phase sensitivity of NCO based on the homodyne detection as a function of  $\phi$  with  $\alpha = 1$  and  $g = 1$ . The black solid line corresponds to the standard SU(1,1) interferometer; the red dashed line and the blue dotted line correspond to the PA-then-PS and PS-then-PA, respectively.

Fig. 3 illustrates the phase sensitivity  $\Delta\phi$  plotted against the gain factor  $g$  for different schemes. The plot confirms that an increase in the gain factor  $g$  enhances the phase sensitivity. Additionally, it is observed that the phase sensitivity of both schemes improves more significantly at lower  $g$  values, and the difference between the two schemes initially decreases and then increases with  $g$ . Notably, the PA-then-PS scheme demonstrates higher phase sensitivity than the PS-then-PA scheme across the entire range of  $g$  values.

Similarly, we analyze the phase sensitivity  $\Delta\phi$  as a function of the coherent amplitude  $\alpha$ , as depicted in Fig. 4. The phase sensitivity improves with the coherent amplitude  $\alpha$ , attributed to the increase in the mean photon number with  $\alpha$ , then enhancing intramode correlations and quantum entanglement between the two modes. Furthermore, the enhancement effect diminishes as the coherent amplitude  $\alpha$  increases. It is noteworthy that the PS-then-PA scheme yields higher phase sensitivity than the PA-then-PS scheme at small values of  $\alpha$ , while the reverse is observed at larger values of  $\alpha$ . And

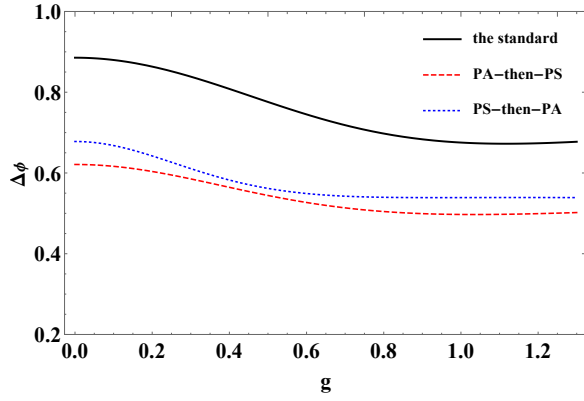


FIG. 3. The phase sensitivity as a function of  $g$ , with  $\alpha = 1$  and  $\phi = 0.6$ .

the optimal phase sensitivity is obtained in the PA-then-PS scheme, again.

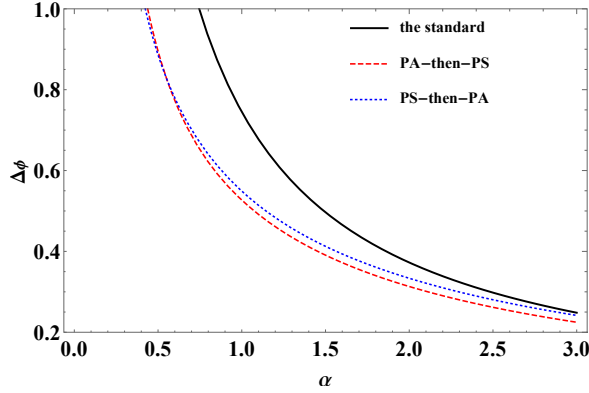


FIG. 4. The phase sensitivity as a function of  $\alpha$ , with  $g = 1$  and  $\phi = 0.6$ .

### B. Photon losses case

The SU(1,1) interferometer plays a critical role in achieving high-precision measurements. However, precision is significantly affected by photon losses, particularly internal losses. Here, we focus on internal photon losses, corresponding to  $T_k \in (0, 1)$ . The phase sensitivity, depicted as a function of transmittance  $T_k$  in Fig. 5 for fixed  $g$ ,  $\alpha$ , and  $\phi$ , improves as anticipated with higher transmittance  $T_k$ . Lower transmittance corresponds to increased internal losses, weakening the performance of phase estimation. Both PA-then-PS and PS-then-PA schemes within the SU(1,1) interferometer effectively enhance the phase sensitivity  $\Delta\phi$ . Moreover, it is notable that as transmittance  $T_k$  increases, the improvement in phase sensitivity first increases and then decreases for both schemes. Notably, the PA-then-PS scheme consistently

demonstrates higher phase sensitivity than the PS-then-PA scheme across the entire range.

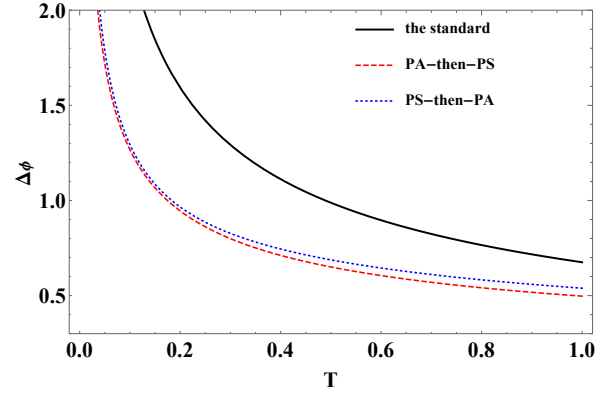


FIG. 5. The phase sensitivity as a function of transmittance  $T_k$ , with  $g = 1$ ,  $\phi = 0.6$  and  $\alpha = 1$ .

### C. Comparison with SQL and HL

Additionally, we compare the phase sensitivity with SQL and HL in this subsection. The SQL and HL are defined as  $\Delta\phi_{SQL} = 1/\sqrt{N}$  and  $\Delta\phi_{HL} = 1/N$ , respectively, where  $N$  represents the total average photon number inside the interferometer before the second OPA for each scheme [64, 65].  $N$  can be calculated as

$$\begin{aligned} N_1 &= A_1^2 \langle \Psi_{in} | U_{S_1}^\dagger U_B^\dagger U_{P_1}^\dagger (a^\dagger a + b^\dagger b) U_{P_1} U_B U_{S_1} | \Psi_{in} \rangle \\ &= A_1^2 (P_{3,3,0,0} + 5P_{2,2,0,0} + 4P_{1,1,0,0} \\ &\quad + P_{2,2,1,1} + 3P_{1,1,1,1} + P_{0,0,1,1}), \end{aligned} \quad (12)$$

for PA-then-PS and

$$\begin{aligned} N_2 &= A_2^2 \langle \Psi_{in} | U_{S_1}^\dagger U_B^\dagger U_{P_2}^\dagger (a^\dagger a + b^\dagger b) U_{P_2} U_B U_{S_1} | \Psi_{in} \rangle \\ &= A_2^2 (P_{3,3,0,0} + 3P_{2,2,0,0} + P_{1,1,0,0} \\ &\quad + P_{2,2,1,1} + P_{1,1,1,1}), \end{aligned} \quad (13)$$

for the PS-then-PA, respectively.

In this subsection, we set the parameters  $g = 0.7$  and  $\alpha = 1$  for all schemes and compare the phase sensitivity  $\Delta\phi$  with the SQL and the HL of the standard SU(1,1) interferometer, as shown in Fig. 6. Our findings demonstrate that (i) the original interferometer (without NCO) cannot surpass the SQL. (ii) Within a wide range, the NCO schemes are capable of surpassing the SQL even in the presence of significant photon losses (Fig. 6(b)). This suggests that the NCO schemes exhibit better robustness against internal photon losses. (iii) It is clear that the PA-then-PS scheme outperforms the PS-then-PA scheme at small phase values, while the opposite is true at large phase values.

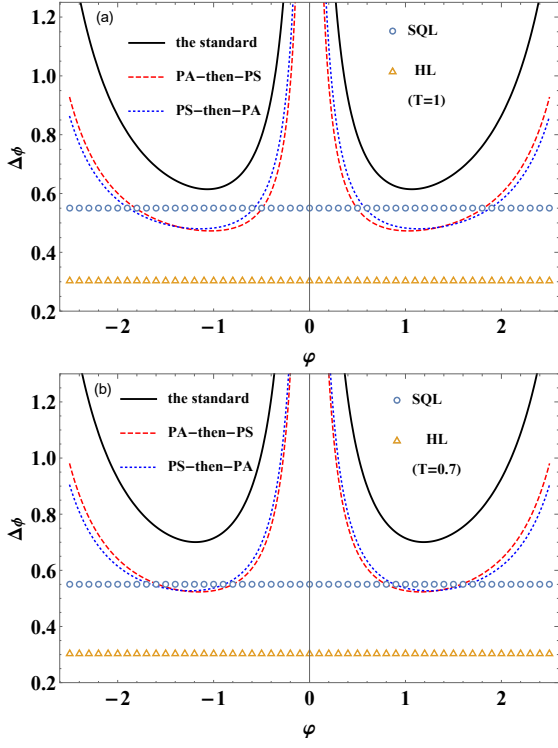


FIG. 6. Comparison of the phase sensitivity with the SQL and HL. The blue circle is the SQL and the yellow triangle is the HL. (a)  $T = 1$ , (b)  $T = 0.7$ .

#### IV. THE QUANTUM FISHER INFORMATION

In the previous discussions, we have explored the influence of NCO schemes on phase sensitivity and the correlation between phase sensitivity and relevant parameters using homodyne detection. It is crucial to recognize that the discussed phase sensitivity is influenced by the chosen measurement method. Hence, the question arises: how can we achieve maximum phase sensitivity in an interferometer that is independent of the measurement method used? This section shifts our focus to the QFI, which represents the maximum information extracted from the interferometer system, regardless of the measurement method employed. We will examine the QFI in ideal and realistic scenarios, respectively.

##### A. Ideal case

For a pure state system, the QFI can be derived by [66]

$$F = 4 \left[ \langle \Psi'_\phi | \Psi'_\phi \rangle - |\langle \Psi'_\phi | \Psi_\phi \rangle|^2 \right], \quad (14)$$

where  $|\Psi_\phi\rangle$  is the quantum state after phase shift and before the second OPA, and  $|\Psi'_\phi\rangle = \partial |\Psi_\phi\rangle / \partial \phi$ . Then

the QFI can be reformed as [66]

$$F = 4 \langle \Delta^2 n_a \rangle, \quad (15)$$

where  $\langle \Delta^2 n_a \rangle = \langle \Psi_\phi | (a^\dagger a)^2 | \Psi_\phi \rangle - (\langle \Psi_\phi | a^\dagger a | \Psi_\phi \rangle)^2$ .

In the ideal NCO, the quantum state is given by  $|\Psi_\phi\rangle = A_j U_\phi U_{P_j} U_{S_1} |\Psi_{in}\rangle$  with  $|\Psi_{in}\rangle = |\alpha\rangle_a \otimes |0\rangle_b$ , and  $U_{P_1} = aa^\dagger$ ,  $U_{P_2} = a^\dagger a$ . Thus, the QFI is derived as

$$F_1 = 4 \{ A_1^2 (P_{4,4,0,0} + 8P_{3,3,0,0} + 14P_{2,2,0,0} + 4P_{1,1,0,0}) - [A_1^2 (P_{3,3,0,0} + 5P_{2,2,0,0} + 4P_{1,1,0,0})]^2 \}, \quad (16)$$

for the PA-then-PS and

$$F_2 = 4 \{ A_2^2 (P_{4,4,0,0} + 6P_{3,3,0,0} + 7P_{2,2,0,0} + P_{1,1,0,0}) - [A_2^2 (P_{3,3,0,0} + 3P_{2,2,0,0} + P_{1,1,0,0})]^2 \}, \quad (17)$$

for the PS-then-PA, respectively. In the above equations,  $T_k = 1$ . It is possible to explore the connection between the QFI and the related parameters using Eqs. (16) and (17).

Figs. 7 and 8 illustrate the QFI as a function of  $g$  ( $\alpha$ ) for a specific  $\alpha$  ( $g$ ). It is evident that a higher value of  $g$  ( $\alpha$ ) corresponds to a greater QFI. Both the PA-then-PS and PS-then-PA result in an enhanced QFI due to the non-Gaussian nature. The QFI of PA-then-PS is slightly higher than that of PS-then-PA in both figures. Moreover, we observe that the improvement of QFI due to non-Gaussian operations increases with the increase of the value  $g$  (as shown in Fig. 7), while it does not significantly change with the variation of the value  $\alpha$  (as shown in Fig. 8).

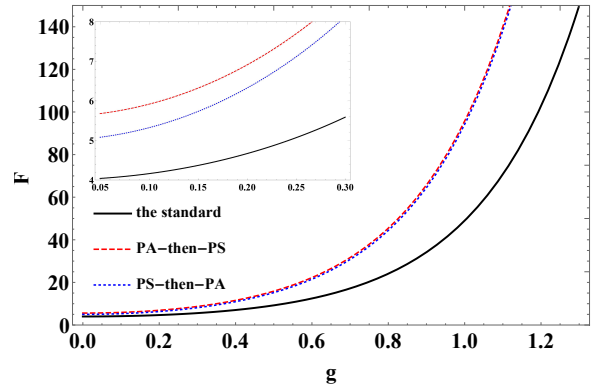


FIG. 7. The QFI as a function of  $g$ , with  $\alpha = 1$ .

Actually, the QFI can be associated with the phase sensitivity through [67]

$$\Delta\phi_{QCRB} = \frac{1}{\sqrt{vF}}, \quad (18)$$

where  $v$  represents the number of measurements, we simplify by setting  $v = 1$ . Another quantum limit, the

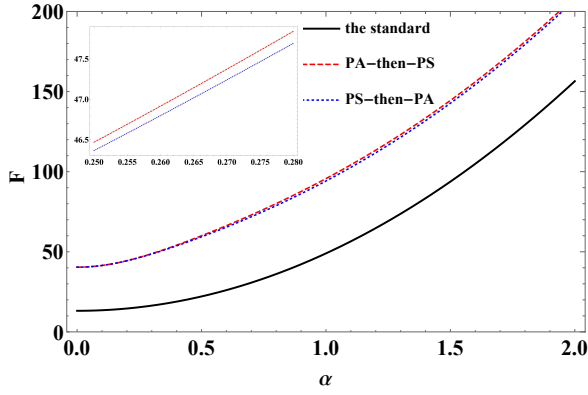


FIG. 8. The QFI as a function of  $\alpha$ , with  $g = 1$ .

QCRB [53, 54], denoted as  $\Delta\phi_{QCRB}$ , defines the ultimate limit for a set of probabilities derived from measurements on a quantum system. It is an estimator implemented asymptotically by a maximum likelihood estimator and provides a detection-independent phase sensitivity.

Fig. 9 and Fig. 10 illustrate the variation of  $\Delta\phi_{QCRB}$  as a function of  $g$  ( $\alpha$ ) for a specific  $\alpha$  ( $g$ ). It is shown that  $\Delta\phi_{QCRB}$  improves with increasing  $g$  and  $\alpha$ . Similarly, due to the non-Gaussian nature, both the PA-then-PS and PS-then-PA are able to improve the  $\Delta\phi_{QCRB}$ . Furthermore, the improvement in  $\Delta\phi_{QCRB}$  is more obvious for small coherent amplitude  $\alpha$  (refer to Fig. 10). Overall, the PA-then-PS exhibits a better performance than the PS-then-PA.

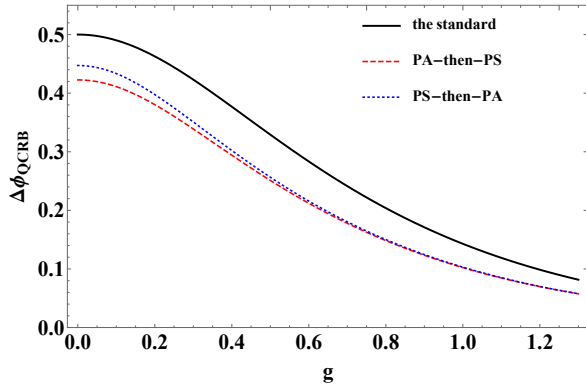


FIG. 9. The  $\Delta\phi_{QCRB}$  as a function of  $g$ , with  $\alpha = 1$ .

### B. Photon losses case

In this subsection, we extend our analysis to cover the QFI in the presence of photon losses. Specifically, we examine homodyne detection on mode  $a$ , which is susceptible to photon losses. Consequently, our attention is directed toward the QFI of the system with photon losses

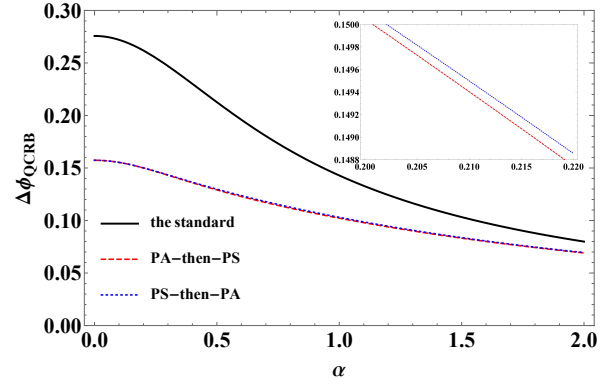


FIG. 10. The  $\Delta\phi_{QCRB}$  as a function of  $\alpha$ , with  $g = 1$ .

in mode  $a$ , as depicted in Fig. 11. For realistic quantum systems, we have demonstrated the feasibility of computing the QFI with internal non-Gaussian operations by redefining the Kraus operator according to the method proposed by Escher *et al.* [66]. The method can be summarized as follows.

In an expanded space, the pure state  $|\psi\rangle = U_{S1}|\alpha\rangle_a|0\rangle_b$  is the correlated probe state after the input state  $|\alpha\rangle_a \otimes |0\rangle_b$  is injected into the first OPA of SU(1,1) interferometer. According to Ref. [66], the quantum state  $|\psi\rangle$  of the input system can be described by the Kraus operators after undergoing photon losses, resulting in the quantum state  $|\Psi_S\rangle$  as follow

$$\begin{aligned} |\Psi_S\rangle &= B_{1,2} U_{S,E} |\psi\rangle |0\rangle_E \\ &= B_{1,2} \sum_l \hat{\Pi}_l(\phi, \eta, \alpha) |\psi\rangle |0\rangle_E, \end{aligned} \quad (19)$$

where  $\hat{\Pi}_l(\phi, \eta, \alpha)$  is the new Kraus operator,  $B_{1,2}$  is the normalization factor, and  $|0\rangle_E$  represents vacuum noise. Thus, for the whole purified system, the QFI turns out to be

$$\begin{aligned} F_L &\leq C_Q \left[ |\psi\rangle, \hat{\Pi}_l(\phi, \eta, \lambda) \right] \\ &= 4 \left[ \langle \psi | \hat{H}_1 | \psi \rangle - \left| \langle \psi | \hat{H}_2 | \psi \rangle \right|^2 \right], \end{aligned} \quad (20)$$

where Hermitian operators  $\hat{H}_{1,2}$  are defined by

$$\hat{H}_1 = \sum_l \frac{d\hat{\Pi}_l^\dagger(\phi, \eta, \lambda)}{d\phi} \frac{d\hat{\Pi}_l(\phi, \eta, \lambda)}{d\phi}, \quad (21)$$

$$\hat{H}_2 = i \sum_l \frac{d\hat{\Pi}_l^\dagger(\phi, \eta, \lambda)}{d\phi} \hat{\Pi}_l(\phi, \eta, \lambda). \quad (22)$$

Therefore, by finding the minimum value of  $C_Q \left[ |\psi\rangle, \hat{\Pi}_l(\phi, \eta, \lambda) \right]$  using Eq. (20), we can obtain the QFI of the SU(1,1) interferometer based on internal non-Gaussian operations under photon losses.

Next, we analyze the QFI of the NCO schemes with the photon losses occurring before the NCO and after the



phase shifter in the mode  $a$ , as shown in Fig. 11. Subsequently, we can get the new Kraus operators  $\hat{\Pi}_{l_1}(\phi, \eta, \lambda)$  and  $\hat{\Pi}_{l_2}(\phi, \eta, \lambda)$  for the PA-then-PS and the PS-then-PA, respectively, i.e.,

$$\hat{\Pi}_{l_1}(\phi, \eta, \lambda) = B_1 \sqrt{\frac{(1-\eta)^l}{l!}} e^{i\phi(n-\lambda)} \eta^{\frac{n}{2}} \times a^l [aa^\dagger - (1+\lambda)l], \quad (23)$$

and

$$\hat{\Pi}_{l_2}(\phi, \eta, \lambda) = B_2 \sqrt{\frac{(1-\eta)^l}{l!}} e^{i\phi(n-\lambda)} \eta^{\frac{n}{2}} \times a^l [a^\dagger a - (1+\lambda)l], \quad (24)$$

where  $\lambda = 0$  and  $\lambda = -1$  represent the photon losses before the NCO and after the phase shifter, respectively.  $\eta$  is related to the dissipation factor with  $\eta = 1$  and  $\eta = 0$  being the cases of complete lossless and absorption, respectively.  $B_1$  and  $B_2$  are the normalization constants for the PA-then-PS and PS-then-PA, respectively.  $n$  is the particle number operator.

Thus, we can obtain the QFI for non-Gaussian operation inside the interferometer under photon losses [24]. The detailed calculations are summarized in Appendix B.

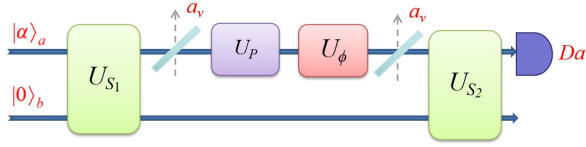


FIG. 11. Schematic diagram of the photon losses on mode  $a$ . The losses occurs before the NCO.

In the presence of photon losses, we analyze the effects of each parameter on the QFI to further characterize the degradation of QFI due to photon losses. An observation from Fig. 12 is that the QFI increases with the rising transmittance  $\eta$ , and the NCO can enhance the QFI. This increase can be attributed to the NCO raising the number of photons internally, resulting in higher quantum information, akin to the ideal case. For both non-Gaussian operations, the improved QFI increases with the transmittance  $\eta$ . Additionally, over a wide range (presumably  $0 < \eta < 0.95$ ), the PS-then-PA exhibits a higher QFI than the PA-then-PS. However, as  $\eta$  approaches 1, the PA-then-PS demonstrates a superior QFI.

Fig. 13 and Fig. 14 illustrate the QFI as a function of  $g$  ( $\alpha$ ) for a given  $\alpha$  ( $g$ ), with  $\eta = 0.7$ . The QFI increases with the rise in  $g$  ( $\alpha$ ), and both non-Gaussian operations can enhance the QFI. The improved QFI is observed to increase with  $g$  (refer to Fig. 13), while improvement decreases with  $\alpha$  (refer to Fig. 14). Moreover, the PA-then-PS scheme performs better than PS-then-PA when  $g$  is smaller, but the opposite is true when  $g$  is larger. However, in the curve showing the variation of  $\alpha$ , the

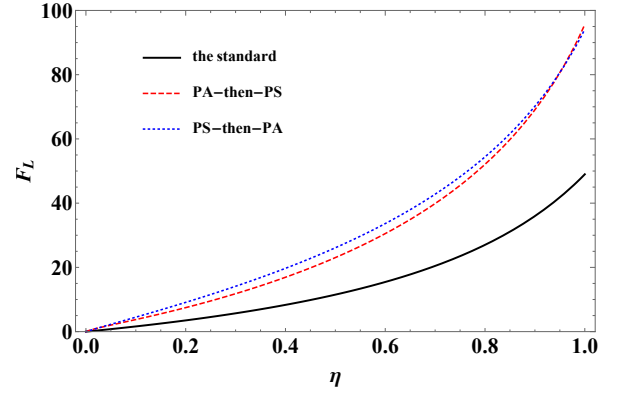


FIG. 12. The  $F_L$  as a function of transmittance  $\eta$ , with  $g = 1$  and  $\alpha = 1$ .

PS-then-PA scheme outperforms the PA-then-PS scheme consistently.

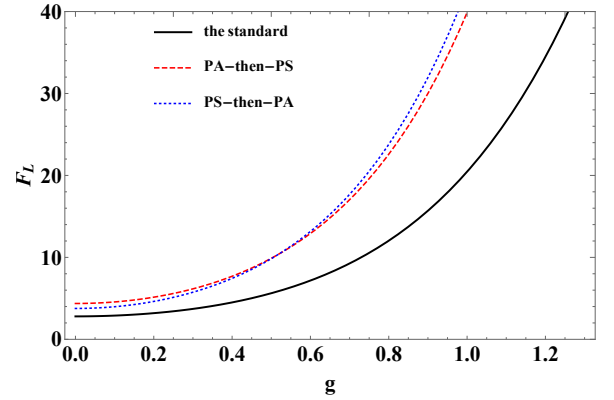


FIG. 13. The  $F_L$  as a function of  $g$ , with  $\alpha = 1$  and  $\eta = 0.7$ .

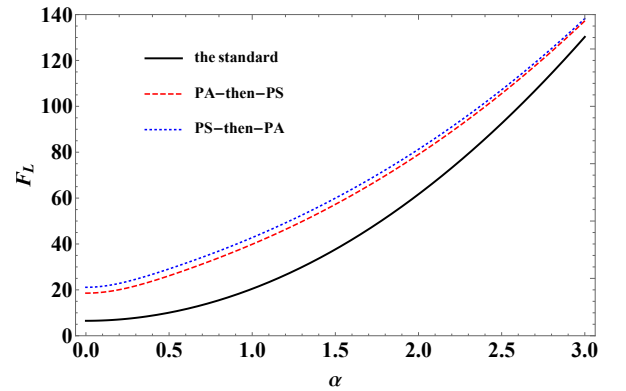


FIG. 14. The  $F_L$  as a function of  $\alpha$ , with  $g = 1$  and  $\eta = 0.7$ .

Similarly to the ideal case, the calculation of  $\Delta\phi_{QCRBL}$  is given by  $\Delta\phi_{QCRBL} = 1/\sqrt{vF_L}$ , with  $v = 1$ . From Fig. 15, it is evident that the  $\Delta\phi_{QCRBL}$  improves as the transmittance  $\eta$  increases, and the improvement initially increases and then decreases. In general, the PS-then-

PA scheme is superior to the PA-then-PS scheme, with the improvement advantage increasing initially and then decreasing as  $\eta$  increases.

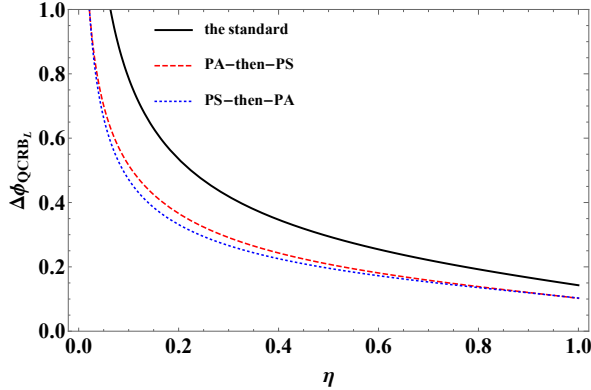


FIG. 15. The  $\Delta\phi_{QCRB_L}$  as a function of transmittance  $\eta$ , with  $g = 1$  and  $\alpha = 1$ .

## V. CONCLUSION

In this paper, we have analyzed the effects of NCO schemes on the phase sensitivity, the QFI and the QCRB in both ideal and real cases. Additionally, we have investigated the effects of the gain coefficient  $g$  of the parametric amplifier, the coherent state amplitude  $\alpha$  and the beam splitter transmittance  $T_k$  on the performance of the system. Through analytical comparison, we have verified that the NCO schemes can improve the measurement accuracy of the SU(1,1) interferometer and enhance the robustness to internal photon losses. The non-Gaussian operations can elevate the total average photon number of the SU(1,1) interferometer, consequently reinforcing intramode correlations and quantum entanglement between the two modes.

We further analyze the disparities between the two non-Gaussian operations. Concerning phase sensitivity, the improvement of the PA-then-PS scheme is superior in both the ideal and photon losses cases. In terms of the QFI and the QCRB, in the ideal case, the PA-then-PS is slightly outperforms the PS-then-PA. However, in the photon losses case, then PS-then-PA demonstrates a greater advantage.

In summary, the NCO schemes play a role in overcoming the internal photon losses in SU(1,1) interferometers and in improving the accuracy of quantum measurements. This study highlights the potential of the non-Gaussian operations as valuable tools for improving the performance of quantum metrology and information processing systems.

## ACKNOWLEDGMENTS

This work is supported by the National Natural Science Foundation of China (Grants No. 11964013 and No. 12104195) and the Training Program for Academic and Technical Leaders of Major Disciplines in Jiangxi Province (No.20204BCJL22053).

## APPENDIX A : THE PHASE SENSITIVITY OF NCO

In this Appendix, we give the calculation formulas of the phase sensitivity in NCO as follows

$$\Delta\phi_1 = \frac{\sqrt{\langle \Psi_{out}^1 | (a^\dagger + a)^2 | \Psi_{out}^1 \rangle - \langle \Psi_{out}^1 | (a^\dagger + a) | \Psi_{out}^1 \rangle^2}}{|\partial \langle \Psi_{out}^1 | (a^\dagger + a) | \Psi_{out}^1 \rangle / \partial \phi|}. \quad (A1)$$

In our paper, the output state  $|\Psi_{out}^1\rangle$  is given by equation (3), so the expectations related to the phase sensitivity in PA-then-PS are specifically calculated as follows [52]

$$\begin{aligned} & \langle \Psi_{out}^1 | (a^\dagger + a) | \Psi_{out}^1 \rangle \\ &= A_1^2 [e^{-i\phi} \cosh g (P_{3,2,0,0} + 4P_{2,1,0,0} + 2P_{1,0,0,0}) \\ & \quad + \sinh g (P_{2,2,0,1} + 3P_{1,1,0,1} + P_{0,0,0,1}) \\ & \quad + e^{i\phi} \cosh g (P_{2,3,0,0} + 4P_{1,2,0,0} + 2P_{0,1,0,0}) \\ & \quad + \sinh g (P_{2,2,1,0} + 3P_{1,1,1,0} + P_{0,0,1,0})], \quad (A2) \end{aligned}$$

and

$$\begin{aligned} & \langle \Psi_{out}^1 | (a^\dagger + a)^2 | \Psi_{out}^1 \rangle \\ &= A_1^2 [e^{-2i\phi} \cosh^2 g (P_{4,2,0,0} + 5P_{3,1,0,0} + 3P_{2,0,0,0}) \\ & \quad + e^{2i\phi} \cosh^2 g (P_{2,4,0,0} + 5P_{1,3,0,0} + 3P_{0,2,0,0}) \\ & \quad + 2 \cosh^2 g (P_{3,3,0,0} + 5P_{2,2,0,0} + 4P_{1,1,0,0}) \\ & \quad + 2e^{-i\phi} \sinh g \cosh g (P_{3,2,0,1} + 4P_{2,1,0,1} \\ & \quad + 2P_{1,0,0,1} + P_{3,2,1,0} + 4P_{2,1,1,0} + 2P_{1,0,1,0}) \\ & \quad + 2e^{i\phi} \sinh g \cosh g (P_{2,3,1,0} + 4P_{1,2,1,0} \\ & \quad + 2P_{0,1,1,0} + P_{2,3,0,1} + 4P_{1,2,0,1} + 2P_{0,1,0,1}) \\ & \quad + \sinh^2 g (P_{2,2,0,2} + 3P_{1,1,0,2} + P_{0,0,0,2} \\ & \quad + P_{2,2,2,0} + 3P_{1,1,2,0} + P_{0,0,2,0} + 2P_{2,2,1,1} \\ & \quad + 6P_{1,1,1,1} + 2P_{0,0,1,1} + 2P_{2,2,0,0} \\ & \quad + 6P_{1,1,0,0} + 2) + A_1^{-2}]. \quad (A3) \end{aligned}$$

The phase sensitivity of the PS-then-PA can be calculated as

$$\Delta\phi_2 = \frac{\sqrt{\langle \Psi_{out}^2 | (a^\dagger + a)^2 | \Psi_{out}^2 \rangle - \langle \Psi_{out}^2 | (a^\dagger + a) | \Psi_{out}^2 \rangle^2}}{|\partial \langle \Psi_{out}^2 | (a^\dagger + a) | \Psi_{out}^2 \rangle / \partial \phi|}, \quad (A4)$$

where the output state  $|\Psi_{out}^2\rangle$  is given by equation (4), and the expectations associated with the phase sensitiv-



ity in PS-then-PA can similarly be calculated as follows

$$\begin{aligned} & \langle \Psi_{out}^2 | (a^\dagger + a) | \Psi_{out}^2 \rangle \\ &= A_2^2 [e^{-i\phi} \cosh g (P_{3,2,0,0} + 2P_{2,1,0,0}) \\ & \quad + \sinh g (P_{2,2,0,1} + P_{1,1,0,1}) \\ & \quad + e^{i\phi} \cosh g (P_{2,3,0,0} + 2P_{1,2,0,0}) \\ & \quad + \sinh g (P_{2,2,1,0} + P_{1,1,1,0})], \end{aligned} \quad (\text{A5})$$

and

$$\begin{aligned} & \langle \Psi_{out}^2 | (a^\dagger + a)^2 | \Psi_{out}^2 \rangle \\ &= A_2^2 [e^{-2i\phi} \cosh^2 g (P_{4,2,0,0} + 3P_{3,1,0,0}) \\ & \quad + e^{2i\phi} \cosh^2 g (P_{2,4,0,0} + 3P_{1,3,0,0}) \\ & \quad + 2 \cosh^2 g (P_{3,3,0,0} + 3P_{2,2,0,0} + P_{1,1,0,0}) \\ & \quad + 2e^{-i\phi} \sinh g \cosh g (P_{3,2,1,0} + 2P_{2,1,1,0} \\ & \quad + P_{3,2,0,1} + 2P_{2,1,0,1}) \\ & \quad + 2e^{i\phi} \sinh g \cosh g (P_{2,3,0,1} + 2P_{1,2,0,1} \\ & \quad + P_{2,3,1,0} + 2P_{1,2,1,0}) \\ & \quad + \sinh^2 g (P_{2,2,2,0} + P_{1,1,2,0} + P_{2,2,0,2} \\ & \quad + 3P_{1,1,0,2} + 2P_{2,2,1,1} + 2P_{1,1,1,1} \\ & \quad + 2P_{2,2,0,0} + 2P_{1,1,0,0}) + A_2^{-2}]. \end{aligned} \quad (\text{A6})$$

## APPENDIX B : THE QFI OF PHOTON LOSSES

We define the new Kraus operators by Eqs. (23) and (24) for the PA-then-PS and the PS-then-PA, respectively. The model satisfies the normalization condition  $Tr \rho = Tr |\Psi\rangle \langle \Psi| = 1$ , i.e.,

$${}_E \langle 0 | \langle \psi | \sum_l^\infty \Pi_l^\dagger(\phi, \eta, \lambda) \Pi_l(\phi, \eta, \lambda) | \psi \rangle | 0 \rangle_E = 1. \quad (\text{B1})$$

Thus, we can then calculate the normalization factors using the following equation

$$B_1 = [\langle \psi | \sum_l^\infty \frac{(1-\eta)^l}{l!} a^{\dagger l} \eta^n (1+n-\lambda)^2 a^l | \psi \rangle]^{-\frac{1}{2}}, \quad (\text{B2})$$

for the PA-then-PS and

$$B_2 = [\langle \psi | \sum_l^\infty \frac{(1-\eta)^l}{l!} a^{\dagger l} \eta^n (n-\lambda)^2 a^l | \psi \rangle]^{-\frac{1}{2}}, \quad (\text{B3})$$

for the PS-then-PA, respectively. Then we can obtain the specific analytic formula for  $B_1$  and  $B_2$ .

$$\begin{aligned} B_1 &= [1 + u_1 (\alpha^2 \cosh^2 r + \sinh^2 r) \\ & \quad + u_2 (\alpha^4 \cosh^4 r + 2 \sinh^4 r) \\ & \quad + 4\alpha^2 \sinh^2 r \cosh^2 r]^{-\frac{1}{2}}, \end{aligned} \quad (\text{B4})$$

where

$$u_1 = 3\eta + 2\lambda\eta - 2\lambda - \lambda^2\eta + \lambda^2, \quad (\text{B5})$$

$$u_2 = 2\lambda\eta^2 - 2\lambda\eta + \eta^2 + \lambda^2\eta^2 - 2\lambda^2\eta + \lambda^2. \quad (\text{B6})$$

And

$$\begin{aligned} B_2 &= [u_{11} * (\alpha^2 \cosh^2 r + \sinh^2 r) \\ & \quad + u_{12} * (\alpha^4 \cosh^4 r + 2 \sinh^4 r) \\ & \quad + 4\alpha^2 \sinh^2 r \cosh^2 r]^{-\frac{1}{2}}, \end{aligned} \quad (\text{B7})$$

where

$$u_{11} = \eta - \lambda^2\eta + \lambda^2, \quad (\text{B8})$$

$$u_{12} = \lambda^2(\eta - 1)^2 + \eta^2 + 2\lambda\eta(\eta - 1). \quad (\text{B9})$$

Using the new Kraus operator, we can derive Eq. (19) to obtain the QFI. In order to derive Eq. (20) using Eq. (23) or Eq. (24), we need to adopt the technique of integrating within an ordered product of operators (IWOP) [68] to derive the operator identity, i.e.,

$$\eta^n n^q =: \frac{\partial^q}{\partial x^q} e^{(\eta e^x - 1)n} |_{x=0}:, \quad (\text{B10})$$

where  $: \cdot :$  indicates the symbol of the normal ordering form, which further leads to the formula

$$\begin{aligned} & \sum_l^\infty \frac{(1-\eta)^l}{l!} l^p a^{\dagger l} \eta^n n^q a^l \\ &= \frac{\partial^{q+p}}{\partial x^q \partial y^p} [\eta e^x + (1-\eta)e^y]^n |_{x=y=0}. \end{aligned} \quad (\text{B11})$$

Using Eq. (B11), the upper bound of the QFI  $C_{Q_1} [|\psi\rangle, \hat{\Pi}_{l_1}(\phi, \eta, \lambda)]$  for the PA-then-PS can be calculated as

$$\begin{aligned} C_{Q_1} [|\psi\rangle, \hat{\Pi}_{l_1}(\phi, \eta, \lambda)] &= 4\{[B_1^2(u_3 \langle \psi | n^4 | \psi \rangle + u_4 \langle \psi | n^3 | \psi \rangle \\ & \quad + u_5 \langle \psi | n^2 | \psi \rangle + u_6 \langle \psi | n | \psi \rangle) \\ & \quad - [B_1^2(u_7 \langle \psi | n^3 | \psi \rangle + u_8 \langle \psi | n^2 | \psi \rangle \\ & \quad + u_9 \langle \psi | n | \psi \rangle)]^2\}, \end{aligned} \quad (\text{B12})$$

where

$$u_3 = (\eta - \lambda + \lambda\eta)^4, \quad (\text{B13})$$

$$\begin{aligned} u_4 &= -2[(\eta - \lambda + \lambda\eta)^2 \\ & \quad \times (3\lambda^2\eta^2 - 3\lambda^2\eta + 6\lambda\eta^2 \\ & \quad - 7\lambda\eta + \lambda + 3\eta^2 - 4\eta)], \end{aligned} \quad (\text{B14})$$

$$\begin{aligned} u_5 &= \lambda^4 (11\eta^4 - 26\eta^3 + 19\eta^2 - 4\eta) \\ & \quad + \lambda^3 (44\eta^4 - 102\eta^3 + 76\eta^2 - 18\eta) \\ & \quad + \lambda^2 (66\eta^4 - 150\eta^3 + 109\eta^2 - 26\eta + 1) \\ & \quad + \lambda (44\eta^4 - 98\eta^3 + 66\eta^2 - 12\eta) \\ & \quad + 11\eta^4 - 24\eta^3 + 14\eta^2, \end{aligned} \quad (\text{B15})$$

$$\begin{aligned}
u_6 &= -\eta(\lambda + 1)^2(\eta - 1) \\
&\quad (6\lambda^2\eta^2 - 6\lambda^2\eta + \lambda^2 \\
&\quad + 12\lambda\eta^2 - 16\lambda\eta + 4\lambda \\
&\quad + 6\eta^2 - 10\eta + 4), \tag{B16}
\end{aligned}$$

$$u_7 = (\eta - \lambda + \lambda\eta)^3, \tag{B17}$$

$$\begin{aligned}
u_8 &= -[\lambda^3(3\eta^3 - 6\eta^2 + 3\eta) + 3\eta^3 \\
&\quad + \lambda^2(9\eta^3 - 17\eta^2 + 10\eta - 2) \\
&\quad + \lambda(9\eta^3 - 16\eta^2 + 7\eta) - 5\eta^2], \tag{B18}
\end{aligned}$$

$$\begin{aligned}
u_9 &= \lambda^3(2\eta^3 - 3\eta^2 + \eta) + 2\eta^3 \\
&\quad + \lambda^2(6\eta^3 - 11\eta^2 + 5\eta) - 5\eta^2 \\
&\quad + \lambda(6\eta^3 - 13\eta^2 + 8\eta - 1) + 4\eta, \tag{B19}
\end{aligned}$$

where  $\langle \cdot \rangle$  is the average under the state  $|\psi\rangle$ , and  $|\psi\rangle = U_{S_1} |\alpha\rangle_a |0\rangle_b$  is the state after the first OPA.  $n$  is the particle number operator. Similarly, we can obtain an upper bound on QFI  $C_{Q_2} [|\psi\rangle, \hat{\Pi}_{l_2}(\phi, \eta, \lambda)]$  for PS-then-PA as

follows

$$\begin{aligned}
C_{Q_2} &[|\psi\rangle, \hat{\Pi}_{l_2}(\phi, \eta, \lambda)] \\
&= 4\{[B_2^2(u_3 \langle \psi | n^4 | \psi \rangle + u_{13} \langle \psi | n^3 | \psi \rangle \\
&\quad + u_{14} \langle \psi | n^2 | \psi \rangle + u_{15} \langle \psi | n | \psi \rangle) \\
&\quad - [B_2^2(u_7 \langle \psi | n^3 | \psi \rangle + u_{16} \langle \psi | n^2 | \psi \rangle \\
&\quad + u_{17} \langle \psi | n | \psi \rangle)]^2\}, \tag{B20}
\end{aligned}$$

where

$$u_{13} = -6\eta(\lambda + 1)^2(\eta - 1)(\eta - \lambda + \lambda\eta)^2, \tag{B21}$$

$$\begin{aligned}
u_{14} &= \eta(\lambda + 1)^3(\eta - 1) \\
&\quad \times (4\lambda - 7\eta - 15\lambda\eta + 11\lambda\eta^2 + 11\eta^2), \tag{B22}
\end{aligned}$$

$$u_{15} = -\eta(\lambda + 1)^4(6\eta^3 - 12\eta^2 + 7\eta - 1), \tag{B23}$$

$$u_{16} = -3\eta(\lambda + 1)^2(\eta - 1)(\eta - \lambda + \lambda\eta), \tag{B24}$$

$$u_{17} = \eta(\lambda + 1)^3(2\eta^2 - 3\eta + 1). \tag{B25}$$

In particular, when  $C_{Q_{1,2}} [|\psi\rangle, \hat{\Pi}_{l_{1,2}}(\phi, \eta, \lambda)]$  reaches the minimum value, it is corresponding to the QFI  $F_{L_{1,2}}$ .

- 
- [1] G. M. D'Ariano and M. G. A. Paris, Arbitrary precision in multipathinterferometry, *Phys. Rev. A* 55, 2267–2271 (1997).
- [2] G. Brida, M. Genovese, and I. R. Berchera, Experimental realization of sub-shot-noise quantum imaging, *Nat. Photonics* 4, 227–230 (2010).
- [3] M. A. Taylor, J. Janousek, V. Daria, J. Knittel, B. Hage, H. A. Bachor, and W. P. Bowen, Biological measurement beyond the quantumlimit, *Nat. Photonics* 7, 229–233 (2013).
- [4] T. Ono, R. Okamoto, and S. Takeuchi, An entanglement-enhancedmicroscope, *Nat. Commun.* 4, 2426 (2013).
- [5] R. X. Adhikari, Gravitational radiation detection with laser interferometry, *Rev. Mod. Phys.* 86, 121–151 (2014).
- [6] C. Bonato, M. S. Blok, H. T. Dinani, D. W. Berry, M. L. Markham, D. J. Twitchen, and R. Hanson, Optimized quantum sensing with a singleelectron spin using real-time adaptive measurements, *Nat. Nanotechnol.* 11, 247–252 (2015).
- [7] C. Degen, F. Reinhard, and P. Cappellaro, Quantum sensing, *Rev. Mod. Phys.* 89, 035002 (2017).
- [8] Y. Ma, H. Miao, B. H. Pang, M. Evans, C. Zhao, J. Harms, R. Schnabel, and Y. Chen, Proposal for gravitational-wave detection beyond the standard quantum limit through EPR entanglement, *Nat. Phys.* 13, 776–780 (2017).
- [9] S. Pirandola, B. R. Bardhan, T. Gehring, C. Weedbrook, and S. Lloyd, Advances in photonic quantum sensing, *Nat. Photonics* 12, 724–733 (2018).
- [10] C. M. Caves, Quantum-mechanical noise in an interferometer, *Phys. Rev. D* 23, 1693 (1981).
- [11] V. Giovannetti, S. Lloyd, and L. Maccone, Quantum-enhanced measurements: Beating the standard quantum limit, *Science* 306(5700), 1330–1336 (2004).
- [12] V. Giovannetti, S. Lloyd, and L. Maccone, Advances in quantum metrology, *Nat. Photonics* 5(4), 222–229 (2011).
- [13] A. N. Boto, P. Kok, D. S. Abrams, S. L. Braunstein, C. P. Williams, and J. P. Dowling, Quantum interferometric optical lithography: exploiting entanglement to beat the diffraction limit, *Phys. Rev. Lett.* 85, 2733 (2000).
- [14] J. P. Dowling, Quantum optical metrology - the low-down on high-NOON states, *Contemp. Phys.* 49(2), 125–143 (2008).
- [15] R. A. Campos, Christopher C. Gerry, and A. Benmoussa, Optical interferometry at the Heisenberg limit with twin Fock states and parity measurements, *Phys. Rev. A* 68, 023810 (2003).
- [16] P. M. Anisimov, G. M. Raterman, A. Chiruvelli, W. N. Plick, S. D. Huver, H. Lee, and J. P. Dowling, Quantum Metrology with Two-Mode Squeezed Vacuum: Parity Detection Beats the Heisenberg Limit, *Phys. Rev. Lett.* 104, 103602 (2010).
- [17] J. Liu, T. Shao, Y. X. Wang, M. M. Zhang, Y. Y. Hu, D. X. Chen, and D. Wei, Enhancement of the phase sensitivity with two-mode squeezed coherent state based on a MachZehnder interferometer, *Opt. Express* 31, 27735

- (2023).
- [18] T. Nagata, R. Okamoto, J. L. Obrien, K. Sasaki, and S. Takeuchi, Beating the Standard Quantum Limit with Four-Entangled Photons, *Science*, **316**, 726 (2007).
- [19] Z. K. Zhao, H. Zhang, Y. B. Huang, and L. Y. Hu, Phase estimation of a Mach-Zehnder interferometer via the Laguerre excitation squeezed state, *Opt. Express* **31**, 17645(2023).
- [20] M. V. Chekhova and Z. Y. Ou, Nonlinear interferometers in quantum optics, *Adv. Opt. Photonics* **8**(1), 104–155(2016).
- [21] Z. Y. Ou and X. Li, Quantum  $su(1, 1)$  interferometers: Basic principles and applications, *APL Photonics* **5**(8), 080902 (2020).
- [22] B. Yurke, S. L. McCall, and J. R. Klauder,  $SU(2)$  and  $SU(1,1)$  interferometers, *Phys. Rev. A* **33**(6), 4033–4054(1986).
- [23] S. K. Chang, C. P. Wei, H. Zhang, Y. Xia, W. Ye, and L. Y. Hu, Enhanced phase sensitivity with a nonconventional interferometer and nonlinear phase shifter, *Phys. Lett. A* **384**(29), 126755 (2020).
- [24] S. K. Chang, W. Ye, H. Zhang, L. Y. Hu, J. H. Huang, and S. Q. Liu, Improvement of phase sensitivity in an  $SU(1, 1)$  interferometer via a phase shift induced by a Kerr medium, *Phys. Rev. A* **105**(3), 033704 (2022).
- [25] C. M. Caves, Reframing  $SU(1,1)$  interferometry, *Adv. Quantum Technol.* **3**(11), 1900138 (2020).
- [26] D. Scharwald, T. Meier, and P. R. Sharapova, Phase sensitivity of spatially broadband high-gain  $SU(1,1)$  interferometers, *Phys. Rev. Research* **5**, 043158 (2023).
- [27] F. Hudelist, J. Kong, C. J. Liu, J. T. Jing, Z. Y. Ou, and W. P. Zhang, Quantum metrology with parametric amplifier-based photon correlation interferometers, *Nat. Commun.* **5**(1), 3049 (2014).
- [28] J. Jing, C. Liu, Z. Zhou, Z. Y. Ou, and W. Zhang, Realization of a nonlinear interferometer with parametric amplifiers, *Appl. Phys. Lett.* **99**(1), 011110 (2011).
- [29] J. Kong, Z. Y. Ou, and W. Zhang, Phase-measurement sensitivity beyond the standard quantum limit in an interferometer consisting of a parametric amplifier and a beam splitter, *Phys. Rev. A* **87**(2), 023825 (2013).
- [30] B. Chen, C. Qiu, S. Chen, J. Guo, L. Q. Chen, Z. Y. Ou, and W. Zhang, Atom-light hybrid interferometer, *Phys. Rev. Lett.* **115**(4), 043602 (2015).
- [31] B. E. Anderson, P. Gupta, B. L. Schmittberger, T. Horrom, C. Hermann-Avigliano, K. M. Jones, and P. D. Lett, Phase sensing beyond the standard quantum limit with a variation on the  $SU(1, 1)$  interferometer, *Optica* **4**(7), 752–756 (2017).
- [32] S. S. Szigeti, R. J. Lewis-Swan, and S. A. Haine, Pumped-up  $SU(1, 1)$  interferometry, *Phys. Rev. Lett.* **118**(15), 150401 (2017).
- [33] G. Frascella, E. E. Mikhailov, N. Takanashi, R. V. Zakharov, O. V. Tikhonova, and M. V. Chekhova, Wide-field  $SU(1,1)$  interferometer, *Optica* **6**(9), 1233–1236 (2019).
- [34] J. Liu, Y. Wang, M. Zhang, J. Wang, D. Wei, and H. Gao, Ultra-sensitive phase measurement based on an  $SU(1, 1)$  interferometer employing external resources and subtract intensity detection, *Opt. Express* **28**(26), 39443–39452 (2020).
- [35] W. Du, J. F. Chen, Z. Y. Ou, and W. Zhang, Quantum dense metrology by an  $SU(2)$ -in- $SU(1, 1)$  nested interferometer, *Appl. Phys. Lett.* **117**(2), 024003 (2020).
- [36] D. Liao, J. Xin, and J. Jing, Nonlinear interferometer based on two-port feedback nondegenerate optical parametric amplification, *Opt. Commun.* **496**, 127137 (2021).
- [37] J.-D. Zhang, C. You, C. Li, and S. Wang, Phase sensitivity approaching the quantum Cramér-Rao bound in a modified  $SU(1,1)$  interferometer, *Phys. Rev. A* **103**, 032617 (2021).
- [38] H. Ma and Y. Liu, Super-resolution localization microscopy: Toward high throughput, high quality, and low cost, *APL Photonics* **5**(6), 080902 (2020).
- [39] Y. K. Xu, S. K. Chang, C. J. Liu, L. Y. Hu, and S. Q. Liu, Phase estimation of an  $SU(1,1)$  interferometer with a coherent superposition squeezed vacuum in a realistic case, *Opt. Express* **30**, 38178 (2022).
- [40] A. M. Marino, N. V. Corzo Trejo, and P. D. Lett, Effect of losses on the performance of an  $SU(1,1)$  interferometer, *Phys. Rev. A* **86**(2), 023844 (2012).
- [41] Z. Y. Ou, Enhancement of the phase-measurement sensitivity beyond the standard quantum limit by a nonlinear interferometer, *Phys. Rev. A* **85**(2), 023815 (2012).
- [42] L. Y. Hu, X. X. Xu, Z. S. Wang, X. F. Xu, Photon-subtracted squeezed thermal state: nonclassicality and decoherence, *Phys. Rev. A* **82**, 043842 (2010).
- [43] L. Y. Hu, M. Al-amri, Z. Y. Liao, M. S. Zubairy, Entanglement improvement via a quantum scissor in a realistic environment, *Phys. Rev. A* **100**, 052322 (2019).
- [44] L. Y. Hu, Z. Y. Liao, M. S. Zubairy, Continuous-variable entanglement via multiphoton catalysis, *Phys. Rev. A* **95**, 012310 (2017).
- [45] H. Zhang, W. Ye, Y. Xia, S. K. Chang, C. P. Wei, L. Y. Hu, Improvement of the entanglement properties for entangled states using a superposition of number-conserving operations, *Laser Phys. Lett.* **16**, 085204 (2019).
- [46] N. Namekata, Y. Takahashi, G. Fujii, D. Fukuda, S. Kurimura, S. Inoue, Non-Gaussian operation based on photon subtraction using a photon-number-resolving detector at a telecommunications wavelength, *Nat. Photon.* **4**, 655–660 (2010).
- [47] A. Zavatta, V. Parigi, M. Bellini, Experimental nonclassicality of single-photon-added thermal light states. *Phys. Rev. A* **75**, 052106 (2007).
- [48] V. Parigi, A. Zavatta, M. Kim, M. Bellini, Probing quantum commutation rules by addition and subtraction of single photons to/from a light field, *Science* **317**, 1890–1893 (2007).
- [49] W. Ye, H. Zhong, Q. Liao, D. Huang, L. Y. Hu, Y. Guo, Improvement of self-referenced continuous variable quantum key distribution with quantum photon catalysis, *Opt. Express* **27**, 17186–17198 (2019).
- [50] K. Zhang, Y. Lv, Y. Guo, J. Jing, and W.-M. Liu, Enhancing the precision of a phase measurement through phase-sensitive non-Gaussianity, *Phys. Rev. A* **105**, 042607 (2022).
- [51] A. Zavatta, V. Parigi, M. S. Kim, H. Jeong, and M. Bellini, Experimental demonstration of the Bosonic commutation relation via superpositions of quantum operations on thermal light fields, *Phys. Rev. Lett.* **103**(14), 140406 (2009).
- [52] Y. K. Xu, T. Zhao, Q. Q. Kang, C. J. Liu, L. Y. Hu, and S. Liu, Phase sensitivity of an  $SU(1,1)$  interferometer in photon-loss via photon operations, *Opt. Express* **31**(5), 8414 (2023).
- [53] C. W. Helstrom, Minimum mean-squared error of estimates in quantum statistics, *Phys. Lett. A* **25**(2), 101 (1967).

- [54] C. W. Helstrom, Quantum detection and estimation theory, *J. Stat. Phys.* 1(2), 231 (1969).
- [55] M. Xiao, L. A. Wu, and H. J. Kimble, Precision measurement beyond the shot-noise limit, *Phys. Rev. Lett.* 59(3), 278 (1987).
- [56] R. Demkowicz-Dobrzański, M. Jarzyna, and J. Kołodyński, Quantum limits in optical interferometry, *Prog. Optics* 60, 345-435 (2015).
- [57] M. Bradshaw, P. K. Lam, and S. M. Assad, Ultimate precision of joint quadrature parameter estimation with a Gaussian probe, *Phys. Rev. A* 97(1), 012106 (2018).
- [58] D. Li, C. H. Yuan, Z. Y. Ou, and W. Zhang, The phase sensitivity of an SU(1,1) interferometer with coherent and squeezed-vacuum light, *New J. Phys* 16(7), 073020 (2014).
- [59] X. Y. Hu, C. P. Wei, Y. F. Yu, and Z. M. Zhang, Enhanced phase sensitivity of an SU(1,1) interferometer with displaced squeezed vacuum light, *Front. Phys.* 11(3), 114203 (2016).
- [60] P. M. Anisimov, G. M. Raterman, A. Chiruvelli, W. N. Plick, S. D. Huver, H. Lee, and J. P. Dowling, Quantum metrology with two-mode squeezed vacuum: parity detection beats the Heisenberg limit, *Phys. Rev. Lett.* 104(10), 103602 (2010).
- [61] D. Li, B. T. Gard, Y. Gao, C. H. Yuan, W. Zhang, H. Lee, and J. P. Dowling, Phase sensitivity at the Heisenberg limit in an SU(1,1) interferometer via parity detection, *Phys. Rev. A* 94(6), 063840 (2016).
- [62] S. Ataman, A. Preda, and R. Ionicioiu, Phase sensitivity of a Mach-Zehnder interferometer with single-intensity and difference-intensity detection, *Phys. Rev. A* 98(4), 043856 (2018).
- [63] D. Li, C. H. Yuan, Y. Yao, W. Jiang, M. Li, and W. Zhang, Effects of loss on the phase sensitivity with parity detection in an SU(1,1) interferometer, *J. Opt. Soc. Am. B* 35(5), 309106 (2018).
- [64] C. M. Caves, Quantum-mechanical noise in an interferometer, *Phys. Rev. D* 23(8), 1693 (1981).
- [65] J. Beltran and A. Luis, Breaking the Heisenberg limit with inefficient detectors, *Phys. Rev. A* 72(4), 045801 (2005).
- [66] B. M. Escher, R. L. de Matos Filho, and L. Davidovich, General framework for estimating the ultimate precision limit in noisy quantum-enhanced metrology, *Nat. Phys.* 7(5), 406 (2011).
- [67] C. W. Helstrom, *Quantum detection and estimation theory* (Academic, 1976), 123.
- [68] H. Y. Fan, H. L. Lu, and Y. Fan, Newton-Leibniz integration for ket-bra operators in quantum mechanics and derivation of entangled state representations, *Ann. Phys.* 321, 480 (2006).